ISSN 1063-7729, Astronomy Reports, 2012, Vol. 56, No. 6, pp. 410–416. © Pleiades Publishing, Ltd., 2012.
Original Russian Text © A.A. Golovko, I.I. Salakhutdinova, 2012, published in Astronomicheskii Zhurnal, 2012, Vol. 89, No. 6, pp. 458–464.

Fractal Properties of Active Regions

A. A. Golovko* **and I. I. Salakhutdinova**

Institute of Solar-Terrestrial Physics, Siberian Branch of the Russian Academy of Sciences, P.O. Box 291, Irkutsk, 664033 Russia

Received November 22, 2011

Abstract—The dynamics of active regions have been investigated using multi-fractal analysis methods, based on magnetograms of the full solar disk in the 630.2 nm line obtained with the SOLIS vector spectromagnetograph of Kitt Peak Observatory (USA) during 2006–2007 and January 1, 2009–April 12, 2010. The applied method of multi-fractal segmentation reveals the appearance of new magnetic fluxes on the Sun disk. A comparison of these fluxes with flare activity shows that the flares are generated in areas of interaction of emerging fluxes with existing structures.

DOI: 10.1134/S1063772912050034

1. INTRODUCTION

To study the dynamic regimes of possible turbulence in solar active regions, a fractal analysis of narrow-band images of the chromosphere and transition layer was carried out in [1–4]. This approach was motivated by the opportunity of obtaining fundamentally new information based on state-of-the-art digital images of the solar atmosphere with high spatial and temporal resolution. Physically, studies of scaling characteristics rely on the idea of self-organized criticality (SOC) [5]—a special condition of a complex system with many degrees of freedom, where a small perturbation can lead to macroscopic reorganization of the whole system. Bak et al. [5] have suggested treating natural, quasi-fractal structures like instantaneous "cross sections" of self-organized critical processes. These structures differ from ideal mathematical fractals, first, in the incompleteness and inaccuracy of the self-similar repetition of the structure and, second, in the limited range over which it is traced. For example, a coastline can be modeled well as a fractal, but only in the range of scales from its full length to the scale of particles of soil. Therefore, when fractal analysis is used in modeling, certain restrictions must taken into account, as in a Fourier analysis.

The technique of fractal analysis of experimental data includes a procedural apparatus, from estimating the fractal dimensions of the object's geometry, taking into account their relation to the Hurst index and spectral index [6–12], to the techniques used to calculate the multi-fractal parameters of the physical fields. These techniques include the use of structure functions [1, 13], Detrended Fluctuation Analysis (DFA), which involves the development of a one-dimensional random-walk model [14], the Wavelet Transform Modulus Maxima (WTMM) technique, which is based on the wavelet transform [15], the use of moments of the partitioning function, and the micro-canonical technique of multi-fractal segmentation [16–19].

In our earlier papers [1–4], we investigated the fractal properties of the intensities in some spectral lines of the solar chromosphere and of the magnetic fields of solar active regions using structure functions, multi-fractal spectra, and the multi-fractal segmentation. The general scheme for each of these methods is the same. In the first step, the selected measure is averaged on all scales; in the second step, the scaling properties are estimated; and, in the third step, the obtained rows or distributions of fractal parameters are analyzed and compared with other results. Some examples of such rows are presented in [20].

In the present work, we give preference to multi-fractal segmentation, but take into account results obtained with the other approaches as well. The main purpose of this study was to create a method for identifying new magnetic flux based on the scaling properties of the magnetic-field distribution. The emergence of an active region is traditionally associated with the emergence from sub-photospheric layers of a system of magnetic ropes that forms part of the overall toroidal magnetic field of the Sun, and its unfolding in the solar atmosphere [21]. This idea has been confirmed by recent studies of horizontal photospheric magnetic fields [22]. The rate of emergence of new magnetic flux can differ [23], and the character of its interaction with the existing photospheric magnetic

*E-mail: golovko@iszf.irk.ru

field determines the flare productivity of the active region. This is why the present study is aimed at obtaining diagnostic measurements of the emergence of new magnetic flux based on the scaling parameters of the magnetic-field distribution.

2. OBSERVATIONS

We used magnetograms of the longitudinal field of the solar disk in the 630.2 nm line, which are obtained on a regular basis with the SOLIS vector spectromagnetograph [24] of the Kitt Peak Observatory (USA). In these observations, maps of the Stokes parameters are constructed using 2048 separate scans of the solar image at the entrance slit of the spectrograph. The diameter of one pixel is 1.14″. The longitudinal magnetic field strength is calculated by inverting the spectral-line profile using a program developed the group of the High Altitude Observatory for the Advanced Stokes Polarimeter [25, 26]. The profile of the scattered light is calculated for each pixel in the solar-disk image. We used data for 2006–2007 and January 1, 2010–April 12, 2010. Inspection of the longitudinal magnetograms gives a maximum noise scatter of the magnetic field of about 3 Gauss.

3. DATA PROCESSING

In [1], we studied the behavior of the structure functions of active regions in the pre-flare stage; the existence of multi-fractal properties of the chromosphere medium was shown using the examples of two activity complexes. The fractal parameters estimated from the structure functions describe a studied object statistically as a whole, and it remains unclear what sections of an active region undergo changes that are associated with flares. To answer to this question, we applied other techniques—computation of singularity spectra, first used in solar physics by Lawrence et al. [16], and the micro-canonical method of multi-fractal analysis, developed in [19, 20, 27]. To test how well the results obtained using the two methods were in agreement, we compared the temporal realizations of the scaling of the structure function and the maximum of the Hölder exponent in the multi-fractal spectrum [28]. The good correlation of these two curves for the set of chromospheric filtergrams of active regions considered demonstrates that both these methods provide the information about the fractal properties of the images. By applying multi-fractal segmentation, the sites of repeated flaring were revealed through the presence of sections where the Hausdorff fractal dimension reaches a minimum. In the present work, this same technique is applied to the solar magnetograms.

We have used a version of multi-fractal analysis based on the use of Choquet capacities, described in [27]. A discussion of some methodological questions related to the application of this formalism to the analysis of solar magnetograms can be found in [19, 20].

The observational data considered here are images of the intensity of the solar radiation in a narrow spectral band, presented in gray scale, in the form of rectangular (in the plane of the sky) matrices of pixels with equal coordinate steps in a limited region that is small enough to neglect the curvature of the solar surface. The sum of the gray scale measurements in a limited region is the photometric measure, denoted below as μ_{sum}. However, the photometric measure does not have a density: μ_{sum} does not necessarily have a derivative. The only suitable measure is the full variation of the observed photometric landscape of the field. This variation is estimated as the integral of the modulus of the gradient of μ_{sum} over a limited domain. However, the large variability of the contrast hinders correct calculation of the gradient; this is why it is reasonable to use Choquet capacities [19, 27] (which are the simplest generalization of Borel measures), which need not be additive, but are monotonic. A version of multi-fractal analysis can be constructed for them [27].

We have used a micro-canonical version of multi-fractal analysis, which uses estimates of the regularity indices in a small vicinity of a current point of an image. If the system studied is multi-fractal in the micro-canonical formalism, it is also multi-fractal in a canonical approach [19].

Let us describe briefly the introduction of Choquet capacities as an analogue of a measure, following [19, 27]. A two-dimensional gray-scale image $I(x, y)$ can be represented as a mapping of the intensity distribution of a part of the solar image that has passed through the telescope and is projected on the input window of the CCD camera. $I(x, y)$ is the convolution of the intensity distribution with the CCD gain function. This gain function is usually a Schwartz function, which makes it possible to work with digital images using analysis methods.

The measure μ can be defined in several ways. Let us consider the measure μ_{sum} mentioned above and the Choquet capacity $\mu_{\max}$, equal to the maximum intensity within eight points (by edge and peak) around a current point. Recall that μ_{sum} is defined as the sum of the intensities of the image pixels. This measure has two drawbacks: the discontinuity caused by pixelization of the image, and the absence of monotonic behavior. When the vicinity of the point ε is increased by one unit, which corresponds to two or three layers of neighboring pixels, μ_{sum} can undergo considerable variations. Hence, the rate of change, i.e., the derivative, of μ_{sum} is not stable to changes in the size r of the vicinity considered.

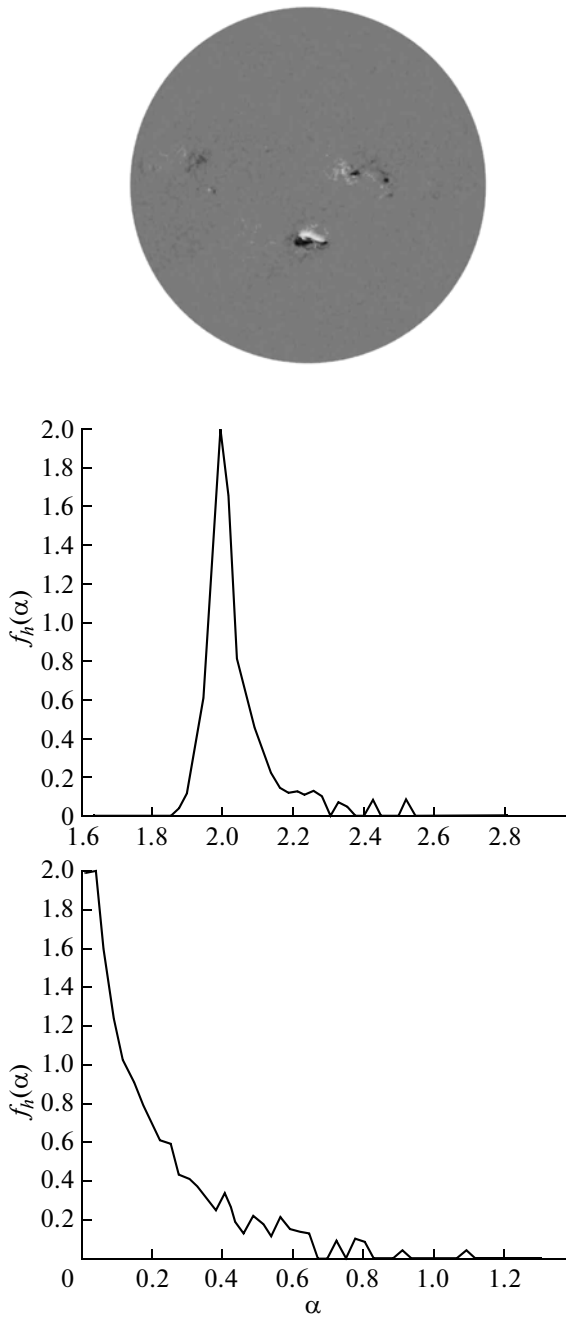

Fig. 1. SOLIS Longitudinal-field magnetogram in the 630.2 nm line (upper), the Hausdorff multi-fractal spectrum $f_h(\alpha)$ for μ_{sum} (middle), and $f_h(\alpha)$ for $\mu_{\max}$ (lower).

This hinders the determination of correct values for the local singularity index from diagrams plotted on a double log scale ($\log \Delta\mu_{sum} - \log r$).

Let us define the Choquet capacity $\mu_{\max}$ for the domain Ω of a digital image as $\mu_{\max}(\Omega) = \max_{I\epsilon\Omega} p(k)$, where $p(k)$ is the intensity of the pixel k.

The quantities μ_{sum} and $\mu_{\max}$ can be used to directly estimate the Hölder exponents α_{sum} and $\alpha_{\max}$, which are the slopes of the linear part of plots of $\log \mu(V_i)$ versus $\log i$. Here, V_i is a square of $i \times i$ pixels, $i = 2n + 1$, $n = 0, 1, 2, \ldots$.

The sense of the multi-fractal singularity spectrum consists of the following [29]. We assume that the distribution of the measure μ (or its analog) is specified on some set. If this set is covered with spheres of diameter ε, then the measure of the sphere centered at the point x_i can be approximated by the power law

$$\mu(\varepsilon) \sim \varepsilon^{\alpha}, \tag{1}$$

where $\alpha = \alpha(x_i)$ is called the singularity exponent, or Hölder exponent. This dependence is usually satisfied in the limit of vanishing scales:

$$\alpha(x_i) = \lim_{\varepsilon \to 0} \ln \mu(\varepsilon) / \ln \varepsilon. \tag{2}$$

The smaller $\alpha(x_i)$, the more "singular" is the measure distribution at the corresponding point is.

For a uniform distribution in a line, $\alpha(x_i) = 1$. Therefore, when $\alpha(x_i) < 1$, the normalized measure $\mu(\varepsilon) \sim \varepsilon^{\alpha-1}$ diverges for sizes of the vicinity close to zero. The limit $\alpha(x_i) = 0$ corresponds to an particle-like measure distribution, similar to a Dirac function, and means that μ is concentrated at individual points.

Each α, given within the limits $(\alpha_k, \alpha_{k+\delta})$, can be compared with the carrier of the measure—the set of points or pixels, in a small vicinity of which the measure has its singularity index within the specified range. It is possible to "measure" this set once its fractal dimension is estimated. The fractal dimension of the set of allocated points can be estimated by covering the figure with set of boxes of various sizes. The minimum number of boxes will be

$$N_\delta(\alpha_k) \approx \delta^{-f(\alpha_k)}. \tag{3}$$

The function $f(\alpha_k)$ is called the Hausdorff, or "box" dimension of the mentioned set of points. As $\delta \to \delta_{\min}$, we obtain the multi-fractal spectrum $f(\alpha)$. Since the spatial resolution of the original image is limited by the diameter of a pixel (a "grain") $\delta_{\min}$, it is usual to call such a spectrum coarse-grained.

The singularity spectrum characterizes the dependence of the number of coverage elements $N_\delta(\alpha)$ on δ, with these elements corresponding to points with singularity exponents equal to some value of α. By definition, f corresponds to the Hausdorff dimension. In the case of a uniform distribution of a measure on the set, $\alpha = \text{const}$, and the singularity spectrum is represented by a single point in the plane (α, f). In the case of a non-uniform distribution of a measure, the function $f(\alpha)$ has the form of an upwards parabola.

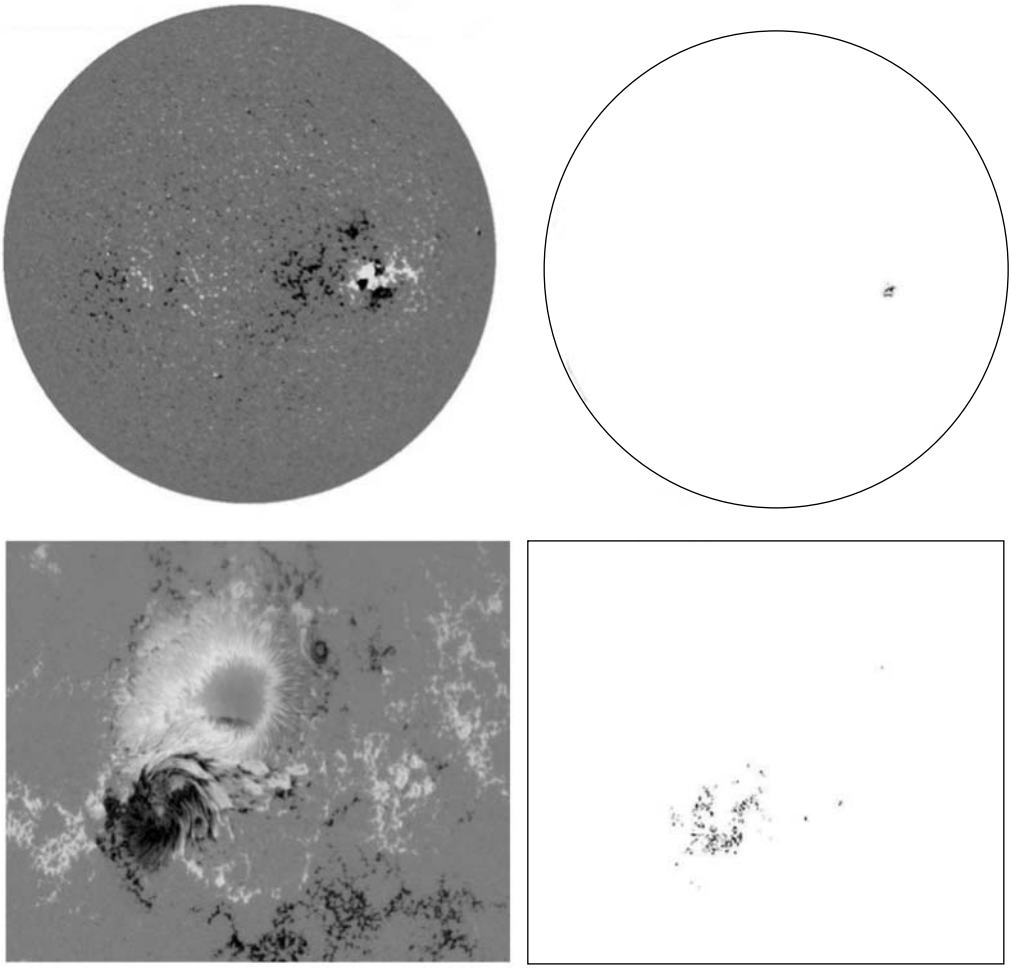

Fig. 2. SOLIS magnetograms (upper) and magnetograms from the HINODE Solar Optical Telescope (lower) for December 13, 2006 (16:10 UT). Segmented images obtained using multi-fractal segmentation for the range of fractal dimension $f = 0{-}0.4$ are shown on the right. These reveal regions of new magnetic flux existing at the current time.

4. RESULTS

In our practical computations, we used the Fraclab software package [30] to calculate the multi-fractal spectra and segmented images. Figure 1 presents the original magnetogram (upper), and the Hausdorff multi-fractal spectra $f(\alpha)$ calculated for the measure μ_{sum} (middle) and the Choquet capacity $\mu_{\max}$ (lower). Spectra were calculated for the whole magnetogram, and are presented here only for positive α. The spectrum for μ_{sum} has the typical shape of a bell [16]. The spectrum for $\mu_{\max}$ is similar to a monotonically falling function—the right half of a Gaussian bell—though for some images in a series it is closer to a straight line, $f = 2 - k\alpha$.

Despite the continuous character of a spectrum $f(\alpha)$, its different parts describe different structures in the original image.

The top of spectrum close to $f = 2$ and $\alpha = 0$ describes smooth sites where the intensity undergoes only small variations from point to point. The area with $f \approx 1$ describes linear objects and sharp edges of features in the image ($f = 1$ for a smooth, one-dimensional line, by definition). The area of f values between one and two is an area of irregular contours and textures. The spectrum here is convex, which corresponds to a multi-fractal character for the conjugate components of the initial distribution. The spectral region below $f = 1$ is more often concave; the structures corresponding to this area require a more detailed study.

The use of the Fraclab package provides the possibility of calculating segmented images corresponding to certain intervals of the fractal dimension f. The apparatus of weakly self-affine functions [31] was used to approximate the distributions in these calculations. Before proceeding to working with magnetograms, we tested this technique on a number of model images, using the spectrum of the maximum values as a

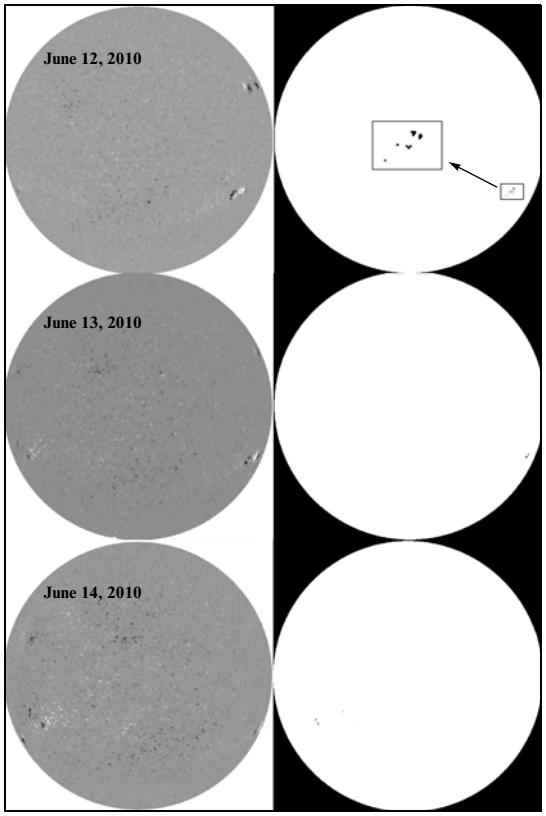

Fig. 3. SOLIS magnetograms for June 12–14, 2010 (left) and the corresponding segmented images (right), which show the locations of regions of new magnetic flux at the corresponding times.

basic spectrum. These computations were carried out separately for positive and negative magnetic-field polarity, and the obtained segmented images were summed. The segmented images for $f = 1.8–2$ revealed smooth sites where the intensity changes little from point to point; the images for $f = 0.9–1.1$ have sharp edges of features ($f = 1$ for a smooth, one-dimensional line). Clusters of small-scale objects appear for $f = 0–0.4$. Since the interpretation of the singularity spectrum is not fully clear for this range, the construction and analysis of the corresponding segmented images were essentially made heuristically, in order to identify significant phenomena at the corresponding sites.

Figure 2 presents the segmented images obtained from SOLIS and HINODE magnetograms for December 13, 2006. These contain patches (clusters of black points) corresponding to fractal dimensions 0–0.4. These patches coincide well with the regions of new emerging flux identified in [32]. The emergence of new flux emergence is confirmed in a movie made from the corresponding magnetograms. This method yields good results in the case of sufficiently high spatial and amplitude (digitization) resolution of the source magnetograms. The spatial sizes of the maximum-singularity patches corresond to those for new magnetic flux at the photosphere level. The interval of scales on which the self-similarity appears provides a good criterion for selection of the maps.

The successful identification of regions of new magnetic flux based on the segmented images suggests that this method could be used as a basis for imaging and the operative publication of maps of the distribution of regions of new magnetic flux on the Sun. Figure 3 presents three SOLIS magnetograms and the corresponding segmented images. Old active regions containing fragmented plages are not visible in the segmented images. On the contrary, young active regions and well-developed active regions in which new magnetic fluxes are developing appear in the segmented images as clusters of black points corresponding to the locations of the regions of new flux. Note that, in principle, the distribution of the Hölder exponent can be used to reveal these clusters, since the hills of the maxima approximately coincide with the clusters in the segmented images.

Time-variation curves for the areas (in millionths of a solar hemisphere, m.s.h.) of regions of new magnetic flux and of sunspots were constructed for eight active regions in the new solar cycle, presented in Fig. 4. These show that the effect of the interaction of new magnetic flux with developed sunspots and plages is visible for the flare-producing sunspot groups 1019, 1045, 1046, and 1054. At the same time, such interaction is essentially is absent from sunspot groups 1027 and 1061, in which there is no flare activity.

5. DISCUSSION AND CONCLUSIONS

Despite the accumulated basis for a model of the evolution of active regions involving the surfacing of magnetic tubes that form part of the overall toroidal magnetic field of the Sun from sub-photospheric layers, there are few means to simultaneously reliably and rapidly identify regions where new magnetic flux emerges. Analyses of time series of magnetograms and intensity images are usually used for this purpose, which is time-consuming. The use of criteria such as enhanced ultraviolet and X ray brightness provides only indirect evidence for the emergence of new magnetic flux.

The method we have proposed here is fast (computation of the segmented images occupies seconds), reliable (it has already been demonstrated using fairly large datasets), and promising (the spatial and peak resolution of the data, as well as speed with which they are delivered, all increase). Its application to data obtained during 2006–2007 and 2009–2010 does not

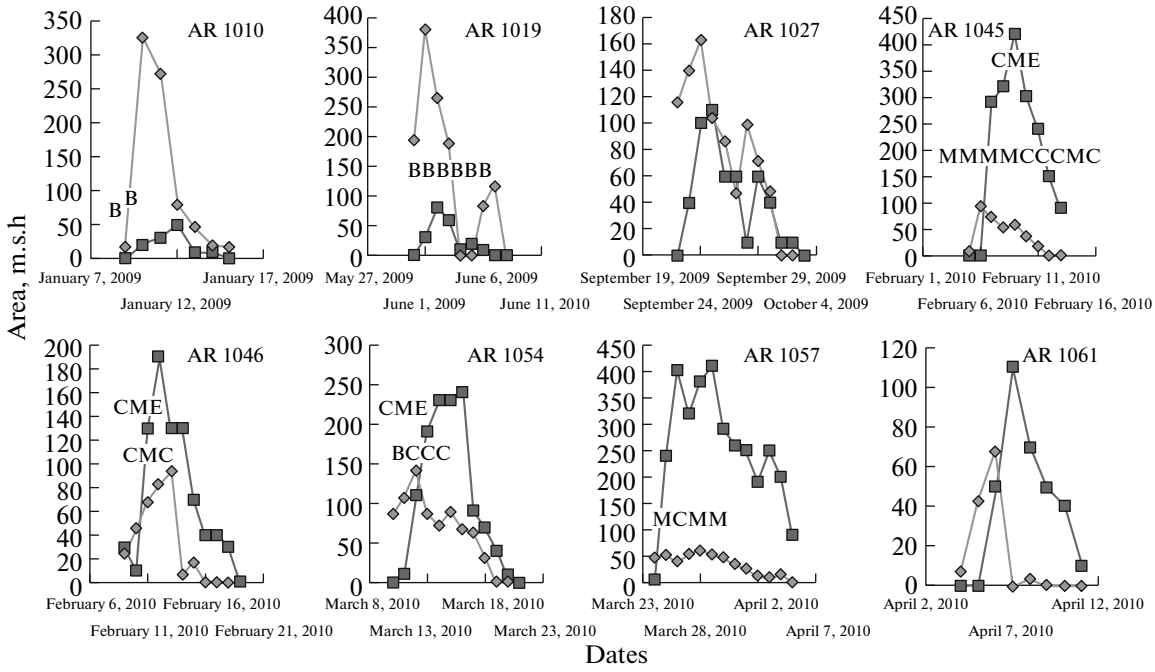

Fig. 4. Temporal variations of the the areas of sunspots (squares) and regions of new magnetic flux (diamonds) in eight active regions during the new solar cycle. The highest X-ray magnitudes of flares are denoted with the letters B, C, M, and coronal-mass ejections are labeled CME.

provide a sufficient test, as there were not many flare-producing regions on the Sun during these times, whereas it is precisely for such regions that the localization of regions of new magnetic flux should yield the most weighty results. Unlike the method used to detect emerging magnetic flux applied in [33], which yielded good results for an active region as a whole, our method is able to localize regions of emerging flux in active regions.

From the point of view of basic research, the existence of special "scaling" properties of regions of new magnetic flux, consisting of the minimum fractal dimensions in these fluxes, may indicate that magnetic-plasma formations that have just emerged carry information about the conditions in sub-photospheric layers, most importantly, the structures of matter flows in these layers.

Our main conclusions are the following.

1. The method of multi-fractal segmentation provides a means of identifying regions of new magnetic flux on the solar disk, based on photospheric magnetograms with high spatial resolution.

2. A comparison of the emergence of new magnetic flux and flare activity shows that flares are generated in areas where new magnetic flux interacts with existing structures. The agreement of this conclusion with known observational results and the standard flare model [34] supports the reliability of the proposed means of identifying regions of new magnetic flux.

ACKNOWLEDGMENTS

This work was supported by the Russian Foundation for Basic Research (grants 11-02-00333a and 11-02-92202_Mong-a), Basic Research Program of the Presidium of the Russian Academy of Sciences No. 4, and the Ministry of Science and Education of the Russian Federation (State Contract No. 02.740.11.0576). We thank Dr. Alexei Pevtsov from Kitt Peak National Observatory, the SOLIS Project scientist, for discussions of questions on techniques for observing and interpreting solar magnetic fields, and also Prof. N.G. Makarenko for useful remarks and discussions. Hinode is a Japanese mission developed and launched by ISAS/JAXA, collaborating with NAOJ as a domestic partner and NASA and STFC (UK) as international partners.

REFERENCES

1. I. I. Salakhutdinova and A. A. Golovko, Sol. Phys. **225**, 59 (2005).
2. A. A. Golovko, I. I. Salakhutdinova, and A. I. Khlystova, Soln.-Zemn. Fiz. **9**, 47 (2006).
3. A. A. Golovko, I. I. Salakhutdinova, and A. I. Khlystova, Geomagn. Aeron. **49**, 907 (2009).
4. A. A. Golovko and I. I. Salakhutdinova, Geomagn. Aeron. **49**, 1084 (2009).

5. P. Bak, C. Tang, and K. Weisenfield, Phys. Rev. A **38**, 364 (1988).
6. J. Feder, *Fractals* (Plenum Press, New York, 1988; Mir, Moscow, 1991).
7. B. Mandelbrot, *The Fractal Geometry of Nature* (W. H. Freeman, New York, 1983), p. 468.
8. I. I. Salakhutdinova, Sol. Phys. **181**, 221 (1998).
9. I. I. Salakhutdinova, Sol. Phys. **188**, 377 (1999).
10. B. A. Ioshpa, V. N. Obridko, and V. E. Chertoprud, Astron. Lett. **33**, 844 (2007).
11. V. I. Abramenko, V. B. Yurchyshin, H. Wang, and P. R. Goode, Astron. Rep. **45**, 824 (2001).
12. V. I. Abramenko, Astron. Rep. **46**, 161 (2002).
13. V. I. Abramenko, V. B. Yurchyshyn, H. Wang, et al., Astrophys. J. **577**, 487 (2002).
14. Gu Gao-Feng and Zhou Wei-Xing, Phys. Rev. E **82**, 011136 (2010).
15. P. Kestener, P. A. Conlon, A. Khalil, et al., Astrophys. J. **717**, 995 (2010).
16. J. K. Lawrence, A. A. Ruzmaikin, and A. C. Cadavid, Astrophys. J. **417**, 805 (1993).
17. J. Levi-Vehel and R. Vojak, Adv. Appl. Math. **20**, 1 (1998).
18. O. A. Kruglun, L. M. Karimova, S. A. Mukhamedzhanova, and N. G. Makarenko, Soln.-Zemn. Fiz. **10**, 31 (2009).
19. N. G. Makarenko and I. S. Knyazeva, Izv. Vyssh. Uchebn. Zaved., Prikl. Nelin. Dinam. **17** (5), 85 (2009).
20. A. A. Golovko and I. I. Salakhutdinova, in *Modern Geodynamics and Dangerous Natural Processes in the Central Azia, Proceedings of the 8th Russian-Mongolian Conference on Astronomy and Geophysics*, Irkutsk, 16–18 Oct. 2009, No. 16, Ed. by K. G. Levi (Inst. Zemnoi Kory SO RAN, Irkutsk, 2010), p. 157.
21. V. M. Grigor'ev, L. V. Ermakova, and A. I. Khlystova, in *Variability of Environment and Climate. Natural and Related Technogenic Catastrophes,* Program No. 16 of Presidium RAS, Vol. 8: *Solar Activity and Physical Processes in Sun-Earth System*, Ed. by N. P. Laverov et al., Collected vol. (Inst. Fiz. Zemli RAN, Moscow, 2008), p. 13 [in Russian].
22. V. A. Sheminova, Astron. Rep. **53**, 477 (2009).
23. A. A. Golovko, Soln.-Zemn. Fiz. **6**, 82 (2004).
24. C. J. Henney, C. U. Keller, and J. W. Harvey, in *Solar Polarization 4*, ASP Conf. Ser. **358**, 92 (2006).
25. A. Skumanich and B. W. Lites, Astrophys. J. **322**, 473 (1987).
26. L. H. Auer, J. N. Heasley, and L. L. House, Sol. Phys. **55**, 47 (1977).
27. J. Levi-Vehel and R. Vojak, Adv. Appl. Math. **20**, 1 (1998).
28. A. A. Golovko and I. I. Salakhutdinova, Soln.-Zemn. Fiz. **13**, 66 (2009).
29. A. N. Pavlov and V. S. Anishchenko, Phys. Usp. **50**, 819 (2007).
30. FRACLAB, A Fractal Analysis Toolbox for Signal and Image Processing, http://fraclab.saclay.inria.fr/.
31. K. Daoudi and J. Levi Vehel, Signal Process. **82**, 2015 (2002).
32. Y. Guo, M. D. Ding, T. Wiegelmann, et al., Astrophys. J. **679**, 1629 (2008).
33. I. S. Knyazeva, N. G. Makarenko, and M. A. Livshits, Astron. Rep. **55**, 463 (2011).
34. K. Shibata, Astrophys. Space Sci. **264**, 129 (1999).

Translated by A. Golovko